Integrating near-edge X-ray absorption fine structure (NEXAFS) microscopy and crystallography: the effects of molecular order

Lisa M. Croll, James F. Britten, Cynthia Morin, Adam P. Hitchcock* and Harald D. H. Stöver

Department of Chemistry and Brockhouse Institute for Materials Research, McMaster University, Hamilton, Ontario, Canada L8S 4M1. E-mail: aph@mcmaster.ca

The carbon *K*-edge near-edge X-ray absorption spectra (NEXAFS) of oriented single crystals of *N*,*N*′′-ethylenebis(*N*′-2-methylphenyl)-urea have been recorded using scanning transmission X-ray microscopy (STXM). The single-crystal structure has been determined by X-ray crystallography. A strong polarization dependence (linear dichroism) has been observed and interpreted with the aid of the single-crystal structure and crystal alignment. These results demonstrate the ability of STXM to determine molecular orientation on a submicrometre spatial scale.

Keywords: NEXAFS microscopy; linear dichroism; X-ray crystallography; phenyl urea.

1. Introduction

New materials are growing increasingly more complex and, as such, chemical and structural characterization by traditional means has become difficult. In many cases, chemical analysis by NMR or IR is inadequate as these techniques do not provide adequate spatial resolution or orientation information. Electron microscopy does provide high spatial resolution, but with only limited chemical speciation. In many cases, chemical composition at high spatial resolution together with information on molecular orientation is desired. For example, in the cases of polymeric liquid-crystal domains formed by *in situ* polymerization-induced phase separation (PIPS) (Nicoletta *et al.*, 2001) of oriented crystalline hydrogen-bonded urea complexes in composite polyurea systems (Etter *et al.*, 1990), and of urea-modified calixarene complexes potentially serving as membrane channels (Hamann *et al.*, 1996), it would be advantageous to obtain both spatially resolved chemical and molecular orientation information.

Scanning transmission X-ray microscopy (STXM) is a recently developed technique (Kirz *et al.*, 1995; Ade, 1998; Ade & Urquhart, 2002) that permits submicrometre chemical speciation through near-edge X-ray absorption fine structure (NEXAFS) spectra recorded with a focused beam of soft X-rays. STXM has previously been used to chemically map polymeric samples with a spatial resolution of about 50 nm (Zhu *et al.*, 1999; Hitchcock, 2001; Koprinarov *et al.*, 2001; Croll *et al.*, 2003). The NEXAFS spectra of anisotropic samples are known to depend on the orientation of the sample relative to the polarization vector of the incident X-rays (Stöhr & Jaeger, 1982; Dudde *et al.*, 1988; Yannoulis *et al.*, 1991; Stöhr, 1992). Polarization-dependent NEXAFS is perhaps best known for studies of molecules adsorbed on single-crystal surfaces (Stöhr, 1992). For 1*s* (*K*-shell) excitations the transition intensity varies according to

$$I \propto \cos^2 \theta, \qquad (1)$$

where θ is the angle between the electric vector of the photon beam (**E**) and the local molecular symmetry axis (**M**), defined as the perpendicular to the bond direction for a carbonyl, and normal to the plane for a phenyl ring (Stöhr & Outka, 1987). Thus the intensity of a $1s \rightarrow \pi^*$ peak is greatest when $\mathbf{E} \parallel \mathbf{M}$. In the case of CO adsorbed on Ni(001), the C $1s \rightarrow \pi^*$ transition is most intense with normal-incidence X-rays where $\mathbf{E} \parallel \mathbf{M}$, and completely disappears at grazing incidence when $\mathbf{E} \perp \mathbf{M}$. Based on this polarization dependence (linear dichroism), one can conclude that the CO molecules are oriented along the normal of the single-crystal Ni surface (Stöhr & Jaeger, 1982). In an analogous experiment, polarization-dependent NEXAFS of anthracene adsorbed onto an Ag(111) surface showed that anthracene lies with its molecular plane parallel to the Ag surface (Yannoulis *et al.*, 1991).

Until now, STXM has been applied mainly to amorphous materials or materials that were not ordered on the scale of the spatial resolution of the beam, and thus the spectra acquired showed no polarization dependence. Exceptions are a STXM study of molecular orientation in Kevlar fibers (Ade & Hsaio, 1993; Smith & Ade, 1996; Ade, 1998) where the orientation of the phenyl rings within fiber cross sections of several tens of micrometres in diameter was clearly demonstrated, and a study of induced orientation in mechanically alloyed polymer blends (Smith *et al.*, 1998). The use of NEXAFS polarization contrast in X-ray microscopy of soft materials is of great interest because it has the potential to determine molecular orientation in materials such as crystalline polymers. Determining molecular orientation on a fine spatial scale (50 nm) is difficult by other methods. Using STXM in such a way would not only allow for determination of the composition of a material, based on its NEXAFS spectrum, but also reveal the spatial distribution of molecular orientation, based on the polarization dependence. This is expected to be very useful in structured nanomaterials and composite systems where it is not possible to generate single crystals suitable for single-crystal X-ray diffraction. Herein we show that NEXAFS spectra can be used to give orientational information about the molecules within crystals of *N*,*N*′′-ethylenebis(*N*′-2-methylphenyl)-urea (bis-urea; see Fig. 1) having dimensions of $\sim 0.1 \times 0.5 \times 10$ µm. Further, we have generated spatial maps of molecular orientation in a cluster of bis-urea crystals.

Bis-urea crystals were selected for this work for a number of reasons. First, the high degree of anisotropic ordering found in these materials makes them an ideal test case for polarization contrast studies. Second, this low-molecular-weight compound contains the relevant structural motif found in polyureas, and was of interest as a reference sample with regard to mapping chemical gradients and molecular orientation in polyurea capsules (Croll *et al.*, 2003). Third, the compound can be fully characterized by traditional methods, including NMR, MS and X-ray crystallography. Finally, the NEXAFS spectra were recorded from single crystals $\sim 0.1 \times 1 \times 10$ µm in size, which illustrates the need for a microscopy-based technique.

2. Experimental

2.1. Materials

All chemicals and solvents used were purchased from Aldrich and used without further purification.

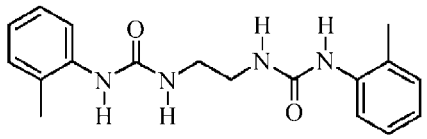

Figure 1
N,*N*′′-ethylenebis(*N*′-2-methylphenyl)urea. Referred to as bis-urea in this paper.

2.2. Synthesis of *N,N′′*-ethylenebis(*N′*-2-methylphenyl)urea

Synthesis of bis-urea was carried out under nitrogen. All apparatus used was dried overnight at 393 K. *o*-Tolyl isocyanate (2.45 g, 0.02 mol) was dissolved in methylene chloride (50 ml). Ethylene diamine (1.12 g, 0.02 mol) was dissolved in methylene chloride (10 ml) in a scintillation vial (20 ml), and 5 ml of this solution was added dropwise by syringe to the stirring isocyanate solution. Immediately upon addition of the amine solution, the urea product started to precipitate from solution. After adding 5 ml of amine solution, addition was paused to add a further 100 ml of methylene chloride to the reaction flask to facilitate mixing. After addition of the remainder of the amine solution, the resulting fine white powder was collected by filtration and rinsed thoroughly with fresh methylene chloride: yield 2.90 g (96.7%); m.p. 522–525 K; 1H-NMR (300 MHz, d6-DMSO) δ 2.17 (*s*, 6H), 3.20 (*d*, 4H), 6.60 (*s*, 2H), 6.86 (*t*, 2H), 7.04–7.11 (*m*, 4H), 7.67 (*s*, 2H), 7.79 (*d*, 2H). 13C NMR (300 MHz, d6-DMSO), δ 17.8, 120.6, 121.9, 125.9, 126.8, 130.0, 138.1, 155.5, the methyl peak at δ 40.1 was hidden beneath the solvent signal and was located using a DEPT experiment. $M_{\rm calculated}$ = 326.4, MS (electrospray), the three most intense peaks are listed: 2M+H 653.3, M+H 327.2, 220.0 (*M* – aminotoluene group). Both 1H-NMR and the melting point correspond to values previously reported in the literature (Guo *et al.*, 1996). The broadness of the melting range is attributed to partial decomposition of the sample at those temperatures.

2.3. Crystallography†

X-ray diffraction data were collected at 173 K on a Mo rotating-anode P4 (Bruker) diffractometer using a SMART 1K CCD detector. A monoclinic unit cell was found, and the structure was determined in $P2_1/c$ by direct phasing and Fourier difference analyses. The molecule was found to have a crystallographic inversion center. The poor unit cell, high *R*-factor, high variance on the weak data, $F_o > F_c$ trend, and noisy difference map indicated twinning. The data were detwinned using GEMINI, and a HKLF5-type file was used in the final F2 refinement (*SHELXTL*). Eight scale factors were used to correct for various degrees of spot overlap. The minor component was determined to be 45% of the sample. H atoms were found in the difference map, and refined isotropically, except for the methyl H atoms which were placed in calculated positions. The principle faces of the crystal were identified.

2.4. STXM

Crystals were cast onto 100 nm-thick Si_3N_4 windows from an ethanol suspension. Images and image sequences were collected using both undulator beamline 7.0.1 STXM and bending-magnet beamline 5.3.2 STXM at the Advanced Light Source (Berkeley, California, USA). STXM images are generated by focusing monochromated plane-polarized soft X-rays using a Fresnel zone plate into a region that has a diameter of ~50 nm over a ~1 µm length along the beam. The sample, which is located at this zone plate focus, is raster scanned perpendicular to the fixed photon beam, while recording the transmitted intensity. Image sequences (a series of such two-dimensional images) are acquired automatically at a fine mesh of energies over the desired energy range. Maps of chemical components are then derived from image sequences by curve fitting of the NEXAFS spectrum at each pixel, or equivalent analyses such as singular value decomposition (Koprinarov *et al.*, 2002). Quantitative mapping is obtained by relating the measured optical density [OD, equation (2), where I_o is the incident X-ray intensity and I is the intensity of the transmitted X-ray beam] to the amount of each constituent through its mass absorption coefficient (equation 2) where $\mu(E)$ is the mass absorption coefficient at a given X-ray energy E, ρ is the density, σ is the linear absorption coefficient and t is the sample thickness.

$$\mathrm{OD} = \ln(I_o/I) = \mu(E)\rho t = \sigma(E)t. \qquad (2)$$

The image sequence used in the present analysis consisted of 110 images between 280 and 305 eV. The separation into the two populations and extraction of pure polarization spectra was performed using *aXis2000*.‡

3. Results and discussion

Bis-urea contains two functional groups with different C $1s \rightarrow \pi^*$ transitions: a carbonyl and phenyl ring which may not have the same spatial orientation of their π^* orbitals. We discuss the orientation of specific bonds or functional groups in terms of the orientation of a local molecular symmetry axis (*M*) with respect to the electric vector of the radiation, instead of the molecular symmetry axis of the molecule as a whole. Fig. 2 shows an STXM image of the bis-urea sample on a Si_3N_4 window recorded at 285 eV. It clearly shows long needle-like crystals oriented both horizontally [hor] and vertically [ver]. Spectra can be extracted from any set of pixels in the image sequence recorded in this area. This allowed us to sample crystals with different spatial orientations thus allowing studies of the NEXAFS polarization dependence without changing the position of

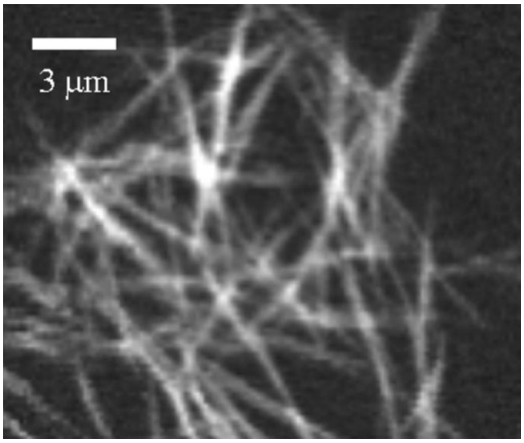

Figure 2
STXM image at 285 eV of the bis-urea crystals recorded at 289.5 eV and converted to OD scale [B = 0, W = 1.6 in optical density (absorbance) units]. The crystals are labelled vertical (ver) or horizontal (hor) based on the direction of the long axis (010) relative to the **E**-vector, which is oriented horizontally.

† CCDC 194850 contains the supplementary crystallographic data for this paper. These data can be obtained free of charge *via* the web at www.ccdc.cam.ac.uk/conts/retrieving.html (or from the CCDC, 12 Union Road, Cambridge CB2 1EZ,UK; fax +44 1223 336033; email: deposit@ccdc.cam.ac.uk). Single-crystal X-ray diffraction analysis at 173 K was carried out on bis-urea ($C_{18}H_{22}N_4O_2$, 326.4 a.m.u.) using a colourless needle-like crystal with dimensions of 0.32 × 0.14 × 0.02 mm. The monoclinic unit cell of bis-urea was determined to be a = 15.02 (3), b = 4.65 (1), c = 11.80 (3), β = 93.36 (7)° with $P2_1/c$ symmetry. There are two formula units in the cell. The crystal was found to be twinned *via* a 180° rotation about *a*, which accounted for the poorly determined cell. The detwinned structure refined to give an agreement factor of 8.23% and a goodness of fit of 0.96.

‡ *aXis2000* is a program for analysis of X-ray images and spectra. It is available from http://unicorn.mcmaster.ca/aXis2000.html.

the sample or the polarization of the beam. Fig. 3 shows the spectra of two crystal orientations: [ver] in which vertically oriented crystals have their long axis perpendicular to the **E**-vector of the light, and [hor] in which horizontally oriented crystals have their long axis parallel to the **E**-vector. The intense peaks at 285.1 eV and 289.5 eV ([ver] spectrum) are assigned to the C 1*s*(ring) $\rightarrow \pi^*_{C=C}$ and C 1*s*(C=O) $\rightarrow \pi^*_{C=O}$ transitions of the phenyl and the carbonyl groups, respectively. The absorption above 290 eV is due to transitions in the aliphatic regions of the molecule. The spectra of the two subpopulations of the crystals in the image sequence are clearly different. The most intense signal in the [ver] spectrum shows an intense C 1*s*(C=O) $\rightarrow \pi^*_{C=O}$ peak at 289.5 eV. This indicates that the carbonyl bond axis in the vertical population of crystals is perpendicular to the **E**-vector. In contrast, the [hor] spectrum shows negligible intensity of the carbonyl peak at 289.5 indicating that in the [hor] population of crystals the carbonyl bond axis lies parallel to the **E**-vector. Since the C 1*s*(C=O) $\rightarrow \pi^*_{C=O}$ transition is completely 'shut off' in the [hor] orientation, both carbonyls within the urea molecule are parallel to one another, and this order is retained consistently throughout the bis-urea crystal.

The C 1*s*(ring) $\rightarrow \pi^*_{C=C}$ transition (285.1 eV) of the phenyl group behaves differently. Its intensity is strongest (relative to the C 1*s* continuum intensity at 300 eV) for the [hor] crystals and it decreases significantly in the [ver] crystals relative to the [hor] spectrum, but it does not disappear completely, irrespective of the crystal orientation relative to the **E**-vector. This behavior of the phenyl signal indicates one of two cases: either the phenyl groups are not completely perpendicular to the **E**-vector in any crystal orientation, or there is more than one orientation of the phenyl rings within the crystal. To confirm these interpretations of the NEXAFS spectra and to determine the exact orientation of the phenyl groups, the single-crystal structure of bis-urea was measured (CCDC 194850 contains the supplementary crystallographic data for this paper).

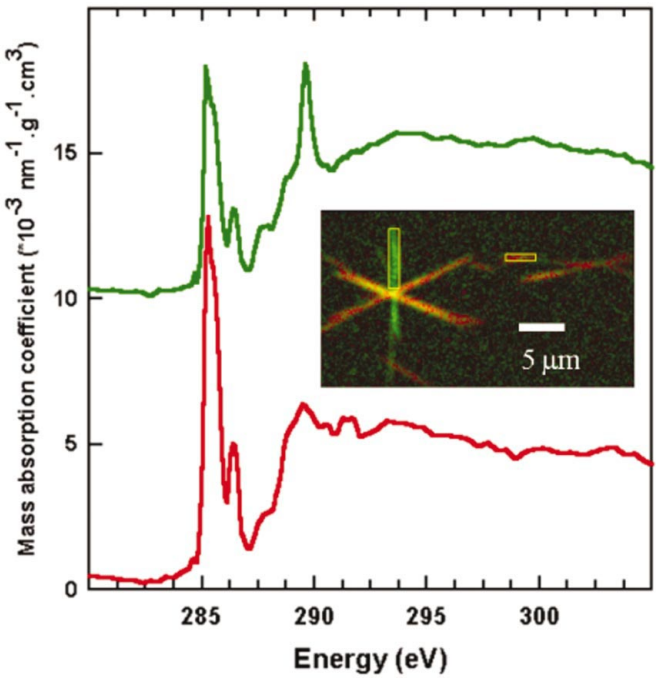

Figure 3
NEXAFS spectra of vertically and horizontally aligned crystals extracted from the regions highlighted with yellow boxes in the insert. The electric vector (**E**) of the linearly polarized X-ray beam was parallel to the horizontal crystals. The insert shows a colour-coded component map derived by singular value decomposition analysis of the full image sequence. Pure red indicates pixels with [hor]-type spectra, pure green indicates pixels with [ver]-type spectra, and shades of yellow arise due the intermediate nature of the spectra of crystals oriented diagonally.

It was determined experimentally that the long dimension of the crystal (corresponding to the direction of fastest growth) was the 010 direction and corresponded to the direction of the one-dimensional hydrogen bonding. The flat face of the crystal is the 100 face or **a** face. All carbonyl groups in the crystal, in spite of the twinning, are aligned approximately parallel to the **b** or 010 (needle) axis as shown in Fig. 4, which shows the view along the 101 direction (the **a**–**c** diagonal). Consequently, in the STXM images (Figs. 2 and 3), the CO bonds of the vertically aligned crystals are also aligned vertically, and those in the horizontally aligned crystals are aligned horizontally, fully explaining the observed intensity variation of the C 1*s*(C=O) $\rightarrow \pi^*_{C=O}$ transition.

Fig. 4 also shows that the phenyl rings in neighbouring molecules adopt two different, nearly orthogonal, orientations in the crystal, which accounts for the fact that it is not possible to 'turn off' the phenyl transition at 285.1 eV in either crystal orientation. The change in the intensity of the C 1*s*(ring) $\rightarrow \pi^*_{C=C}$ transition between the [ver] and [hor] crystals can be explained by considering the angle between the plane of the phenyl ring and the **E**-vector in the two populations. The polarization dependence will differ, depending on whether the crystal is lying on its **a** or **c** face. For the [hor] crystals the angle between **E** and **M** (the normal to the phenyl plane) is 43°, independent of this preference. However, for the [ver] crystals the angle between **E** and **M** is 57° if the crystal is lying on its **a** face, but 63° if the crystal is lying on its **c** face. Thus, the C 1*s*(ring) $\rightarrow \pi^*_{C=C}$ transitions should show a polarization dependence of $[\cos^2(43)/\cos^2(63)] = 2.57$ if the crystal lies on it's **a** face, but a polarization dependence of $[\cos^2(43)/\cos^2(57)] = 1.77$ if the crystal lies on it's **c** face. The ratio of the observed intensities in the spectra of the [hor] and the [ver] crystals is 1.6 (2) for both the undulator and bending-magnet measurements, in agreement with the crystals lying on the **c** face.

4. Summary and outlook

This work has shown that polarization dependence (linear dichroism) can be a powerful contrast mechanism in NEXAFS microscopy. While earlier studies have exploited this effect in studies of naturally aligned materials (Ade & Hsaio, 1993; Smith & Ade, 1996), to our knowledge this is the first example of polarization contrast NEXAFS

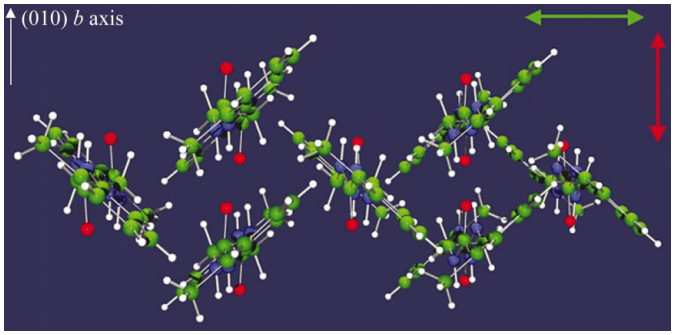

Figure 4
View along the 101 direction of the bis-urea crystal with the 010 direction vertical. This view clearly depicts the parallel arrangement of the carbonyls as well as the alternating alignment of the phenyl rings within the crystal. Note that, for discussion purposes only, two electric vectors ($\mathbf{E}_v$ and $\mathbf{E}_h$) are shown. In the STXM measurements one polarization of the X-rays was used, with two orientations of the crystal.

microscopy of a single-crystal sample for which the orientation has been determined independently and without ambiguity. Polarization-dependent NEXAFS microscopy allows investigation of molecular orientation in single-crystal materials that are not large enough for traditional X-ray diffraction analysis, such as the micrometre-sized crystals investigated in this study (note that the crystal measured by X-ray diffraction was two orders of magnitude larger). Recent advances in insertion-device technology (Young *et al.*, 2002) have enabled rotation of the linear polarization vector. The system at beamline 4.0 at the Advance Light Source allows for orientation of the **E**-vector over a 90° quadrant. A new design, currently being developed at the Canadian Light Source, will allow for full tunability (180° rotation) of the orientation of linearly polarized X-rays. Such control over the polarization of the incident X-ray beam will facilitate orientation analysis of small specific regions of samples. Current procedures to remove, rotate and remount a sample (Smith & Ade, 1996) are very difficult in practice. Coupling a STXM to elliptically polarized undulator light sources will further enhance the ability to interrogate molecular orientation on a submicrometre scale, since neither sample repositioning nor fortuitous sample alignment will be required.

This research was funded by the 3M Canada Company, NSERC (Canada) and the Canada Research Chair program. Thanks are extended to Xiang-Chun Yin and Wen Hui Li for translations of literature and to Paul Zelisko for measuring the NMR spectra. The ALS 7.0.1 STXM was developed by T. Warwick (ALS), B. P. Tonner and collaborators, with support from the US DOE under contract DE-AC03-76SF00098. The 5.3.2 STXM PRT is a ALS-NCSU-McMaster-Dow consortium, led by Harald Ade (NCSU). Seminal contributions in developing this beamline and instrument were made by Harald Ade, David Kilcoyne (NCSU); Tony Warwick, Mike Kritscher, Keith Franck (ALS); Tolek Tyliszczak and Peter Hitchcock (McMaster). Zone plates used at the ALS were provided by Eric Anderson of CXRO, LBNL. We thank ALS staff for much assistance and expert operation

References

Ade, H. (1998). *Experimental Methods in the Physical Sciences* , Vol. 32, p. 225, edited by J. A. R. Samson & D. L. Ederer. New York: Academic Press.
Ade, H. & Hsiao, B. (1993). *Science*, **262**, 1427–1429.
Ade, H. & Urquhart, S. G. (2002). *Chemical Applications of Synchrotron Radiation*, *Advanced Series in Physical Chemistry 12B*, edited by T. K. Sham, pp. 285–355. Singapore: World Scientific.
Croll, L. M., Koprinarov, I., Hitchcock, A. P., Vanbesien, D. & Stöver, H. D. H. (2003). In preparation.
Dudde, R., Frank, K. H. & Koch, E. E. (1988). *J. Electron Spectrosc. Relat. Phenom.* **47**, 245–255.
Etter, M. C., Urbanczyk-Lipkowska, Z., Zia-Ebrahimi, M. & Panunto, T. W. (1990). *J. Am. Chem. Soc.* **112**, 8415–8426.
Guo, D. S., Huang, R. Q., Gao, R. H., Wu, Z. G. & Wang, L. X. (1996). *Chem. J. Chin. Univ.* **17**, 257–261.
Hamann, B. C., Shimizu, K. D. & Rebek, J. Jr (1996). *Angew. Chem. Int. Ed. Engl.* **35**, 1326–1329.
Hitchcock, A. P. (2001). *J. Synchrotron Rad.* **8**, 66–71.
Kirz, J., Jacobsen, C. & Howells, M. Q. (1995). *Rev. Biophys.* **28**, 33–130.
Koprinarov, I., Hitchcock, A. P., Li, W. H., Heng, Y. M. & Stöver, H. D. H. (2001). *Macromolecules*, **34**, 4424–4429.
Koprinarov, I., Hitchcock, A. P., McCrory, C. & Childs, R. F. (2002). *J. Phys. Chem. B*, **106**, 5358–5364.
Nicoletta, F. P., De Filpo, D., Cupelli, D., Macchione, M. & Chidichimo, G. (2001). *Appl. Phys. Lett.* **79**, 4325–4327.
Smith, A. P. & Ade, H. (1996). *Appl. Phys. Lett.* **69**, 3833–3835.
Smith, A. P., Bai, C., Ade, H., Spontak, R. J., Balik, C. M. & Koch, C. C. (1998). *Macromol. Rap. Comm.* **19**, 557–561.
Stöhr, J. (1992). *NEXAFS Spectroscopy*, *Springer Tracts in Surface Science 25.* Berlin: Springer.
Stöhr, J. & Jaeger, R. (1982). *Phys. Rev. B*, **26**, 4111–4131.
Stöhr, J. & Outka, D. (1987). *Phys. Rev. B*, **36**, 7891–7905.
Yannoulis, P., Frank, K. H. & Koch, E. E. (1991). *Surf. Sci.* **241**, 325–334.
Young, A. T., Arenholz, E., Marks, S., Schlueter, R., Steier, C., Padmore, H. A., Hitchcock, A. P. & Castner, D. G. (2002). *J. Synchrotron Rad.* **9**, 270–274.
Zhu, S., Liu, Y., Rafailovich, M. H., Sokolov, J., Gersappe, D., Winesett, D. A. & Ade, H. (1999). *Nature (London)*, **400**, 49–50.

 Received 21 January 2003 • Accepted 25 February 2003